Model for Acoustic Locking of Spin Torque Oscillator

Tanay A. Gosavi
OxideMEMS Lab, Cornell University
Ithaca, NY, USA
tag75@cornell.edu

Sunil A. Bhave
Analog Devices Inc.
Woburn, MA, USA
sunil.bhave@analog.com

***Abstract*—This paper presents a model for locking Spin Torque Oscillator (STO) to an out-of-plane AC strain generated using a mechanical transducer like High-Overtone Bulk Acoustic Resonator (HBAR). We model the magnetization dynamics of the free layer magnet in the STO using the Landau-Lifshitz-Gilbert-Slonczewski (LLGS) equation modified to include magneto-elastic coupling term. Locking is clearly demonstrated from the simulated frequency spectrum of the acoustically-locked STO which has a narrower linewidth and higher signal power as compared to a free running STO. We have shown locking of different modes of the STO and compare the amplitude of out-of-plane AC strain needed to achieve lock. Acoustic locking illustrated here can be used for locking multiple STOs to a common strain transducer and is a potential platform for developing hybrid magneto-acoustic oscillator systems.**

Keywords—Spin Torque Oscillators; Frequency Locking; HBARs, Macro-Spin dynamics

I. INTRODUCTION

STOs are nanoscale GHz frequency self-oscillating magnetic tunnel junctions (MTJ) or spin valve devices [1,2]. In STOs, spin transfer torque generated by spin-polarized electrons overcomes damping in the free layer magnet of the MTJ or spin valve causing steady state precession of the magnetization. Using Tunnel Magneto-Resistance effect (in MTJ) or Giant Magneto-Resistance effect (in Spin Valves) magnetization precession is read out as oscillations of effective impedance of the device. This oscillating impedance modulates the DC bias current to generate an AC current at the frequency of impedance oscillations. STOs have extremely small form factor and octave spanning tuning range but have low output power and poor phase noise limiting their practical use. Locking multiple STOs to a common external reference oscillator has been proposed as a solution and injection locking to a microwave current source has been demonstrated [3]. This scheme improves the output power and reduces the oscillator linewidth but is limited in its ability to lock multiple devices due to problems of impedance mismatch and phase delays between STOs [4]. We believe the challenges in scaling AC current-locked STO systems can be overcome using acoustic locking. Acoustic locking uses inverse magnetostriction effect for generating an effective AC magnetic field in the free layer under the effect of an AC strain applied by a transducer like HBAR [5]. This AC magnetic field which is in phase with transducer drive acts as a locking signal for the STOs narrowing its linewidth and increasing the output power.

This work was supported in part by Cornell Center for Materials Research with funding from NSF MRSEC program (DMR-1120296).

II. MODEL AND SIMULATION SETUP DESCRIPTION

A. LLGS: Macrospin Model of STO

Magnetization dynamics of the free layer of a spin torque oscillator are be modelled using the LLGS equation shown in (1). $\hat{m} = \vec{M}/M_s$ is a unit vector which represents the magnetization $\vec{M}$ of the free layer, where M_s is the saturation magnetization. The first term on the right side of (1) describes the precession of the magnetization $\hat{m}$ around the effective magnetic field $\overrightarrow{H_{eff}}$, where γ is the gyromagnetic ratio of the electron in free layer of the STO.

$$\frac{d\hat{m}}{dt} = -\gamma\hat{m} \times \overrightarrow{H_{eff}} + \alpha\hat{m} \times \frac{d\hat{m}}{dt} + \frac{\gamma\hbar J\eta}{2edM_s}\hat{m} \times (\hat{m} \times \widehat{ep}) \quad (1)$$

The second term on the right side is the damping term, where α is the phenomenological Gilbert damping constant. The effect of the damping term is to relax the magnetization $\hat{m}$ along $\overrightarrow{H_{eff}}$. The value of Gilbert damping constant is material dependent and has origin in magnon-magnon and magnon-phonon scattering [2]. The third term on the right side of (1) is the spin torque term, where J is the current density, ħ is the reduced plank constant, η is the spin polarization efficiency, e is the charge of an electron and d is the thickness of the free layer. Here $\widehat{ep}$ is the spin polarizer vector which is along the direction of the polarizer or the fixed layer magnet in a STO. $\widehat{ep}$ in (1) is used to represent the direction of the spin polarized electrons that are applying a torque to the magnetization of the free layer. Amplitude and the sign of the current density J have direct control over the spin transfer torque amplitude and direction. Increasing the amplitude of bias current the spin torque can overcome the damping in the free layer and result in steady state precession of magnetization.

$$\overrightarrow{H_{eff}} = d\overrightarrow{E_{eff}}/d\hat{m} \quad (2)$$

$$\overrightarrow{H_{eff}} = \overrightarrow{H_{ap}} + H_{an}\hat{n}(\hat{n}.\hat{m}) + H_d\hat{d}(\hat{d}.\hat{m}) + \overrightarrow{H_T} + H_{st}\hat{t}(\hat{t}.\hat{m}) \quad (3)$$

The total effective magnetic field $\overrightarrow{H_{eff}}$ for the free layer magnet is the derivative of its total energy $\overrightarrow{E_{eff}}$ with respect to its magnetization $\hat{m}$ as shown in (2). The components of $\overrightarrow{H_{eff}}$ shown in (3) are derived from constituent energy terms of the magnet. $\overrightarrow{H_{ap}}$ is the external applied magnetic field which is used as a bias field. By varying $\overrightarrow{H_{ap}}$ the frequency of oscillation of the STO can be changed. H_{an} and H_d are the anisotropy and demagnetization fields whose amplitude and

directions ($\hat{n}$ and $\hat{d}$) are dependent on the shape of the magnet [6]. The size and shape of the free layer magnet also determines the initial direction of the magnetization $\hat{m}$. In simulation, direction of magnetization is given in polar coordinates with the azimuthal angle φ and polar angle θ.

B. Thermal Noise in LLGS

The effect of non-zero temperature T and corresponding thermal noise in dynamics of magnetization is accounted via term $\overrightarrow{H_T}$ in (3). $\overrightarrow{H_T}$ is a Gaussian-distributed Langevin term with random direction whose RMS amplitude calculated by fluctuation dissipation argument is shown in (4). In (4) Δt is the simulation step size, V is the volume of the free layer magnet and k_B is the Boltzmann constant [7]. Thermal noise is also accounted for in the model by assuming that the starting azimuthal angle (φ_0) and polar angle (θ_0) of the magnetization have random fluctuations around them. The RMS amplitudes of these thermal fluctuations are calculated using equipartition theorem and are as shown in (5) and (6) for φ_0 and θ_0 respectively.

$$H_T^{RMS} = \sqrt{2\alpha k_B T/\gamma M_s V \Delta t} \quad (4)$$

$$\varphi_0^{RMS} = \sqrt{k_B T/H_{an} M_s V} \quad (5)$$

$$\theta_0^{RMS} = \sqrt{k_B T/H_{ad} M_s V} \quad (6)$$

$$H_{st} = 2B_{eff} S/M_s \quad (7)$$

$$\Delta R = (1 - \hat{m}.\widehat{ep})/2 \quad (8)$$

C. Magneto-Elastic locking term

The effect of out-of-plane strain applied by the HBAR on the free layer magnet is incorporated in the magnetization dynamics as an effective out-of-plane uniaxial shape-anisotropy term H_{st}, which is part of $\overrightarrow{H_{eff}}$ as shown in (3) [5]. Equation (7) gives the amplitude of H_{st}, where B_{eff} is the material dependent magneto-elastic coupling coefficient. Amplitude of H_{st} is proportional to S which is the amplitude of the AC strain along direction $\hat{t}$ acting on the free layer of STO.

D. Simulation Setup

In our simulation of STO we use a MTJ with CoFeB for both free and fixed layer which are separated by MgO based tunnel barrier. The size of the free layer and its relevant magnetic properties taken from [8], are shown in Table I. Applied bias magnetic field and DC bias current amplitude used in simulation are also shown in Table I. For our simulation model with the chosen elliptical shape and size of the free layer the H_{an} field is along the long axis of the magnet in X direction and H_d field which keeps the magnetization from pointing out-of-plane is along the Z direction. The initial direction of magnetization ($\hat{m}$) is along the +X axis. External applied bias field $\overrightarrow{H_{ap}}$ of amplitude 300 Oersted is along the easy axis of the magnet in +X direction as shown in Fig. 1. HBAR as the transducer will generate strain in Z direction which is the out-of-plane direction for the magnet. Thus the magneto-acoustic field due to strain H_{st} will be along the Z direction as shown in Fig. 1. The direction of the polarizer $\widehat{ep}$ is chosen along the +X direction. In the simulation we use step time (Δt) of 10ps, while the total simulation time is

TABLE I. SIMULATION PARAMETERS

Property	Value
Free layer size	$170\ nm \times 100\ nm \times 1.5\ nm$
M_s	$1100\ \mathrm{erg}/cm^3$
H_{an}	$219\ Oe$
H_d	$13000\ Oe$
α	0.01
B_{eff}	$-7 \times 10^7 \mathrm{emu}/cm^3$
η	0.3
H_{ap}	$300\ Oe$
Current Range	1.8 – 8 mA

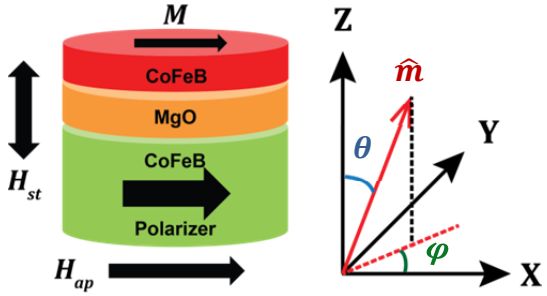

Fig. 1. Directions of M, H_{ap}, H_{st}, Polarizer ($\widehat{ep}$) and the coordinate system used in the simulations.

1μs giving a resolution of up to 2MHz in the extracted frequency spectrum. Simulations were first done without the AC strain S to extract the original spectra of the STO and then were repeated with strain field at the oscillation frequency. The strain field is turned on after the initial 30ns which is sufficient time for magnetization to settle into steady state precession resulting in oscillations of impedance ΔR of STO.

III. EXPERIMENTAL RESULTS AND DISCUSSION

Frequency of the simulated STO changes with the applied bias current as shown in Fig. 2. There are two main regions of operation as seen in Fig. 2 which correspond to two different modes of oscillation for the STO. First mode is the in-plane mode shown in Fig. 3A, where the oscillation frequency decreases with the increasing bias current. Second is when the oscillation frequency increases with the bias current. This mode of oscillation is called the out-of-plane mode (shown in Fig. 3B). As the STO transitions from in-plane mode to out-of-plane mode it goes through a region where the mode has clam-like shape. In this mode the magnetization tilts out-of-plane in both the +Z and –Z directions. The clam-shaped mode (shown in Fig. 3C) is considered as a subset of the in-plane mode as it follows the same frequency-current relation.

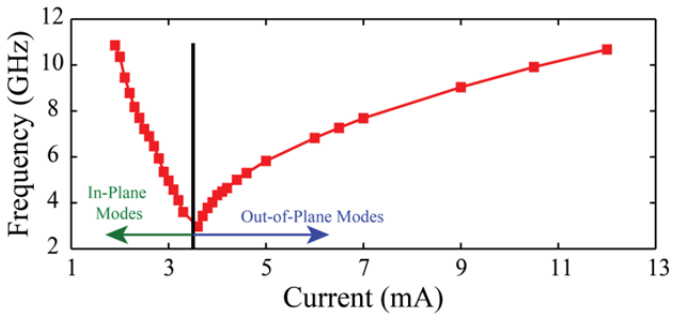

Fig. 2. STO frequency and oscillation mode as a function of bias DC current.

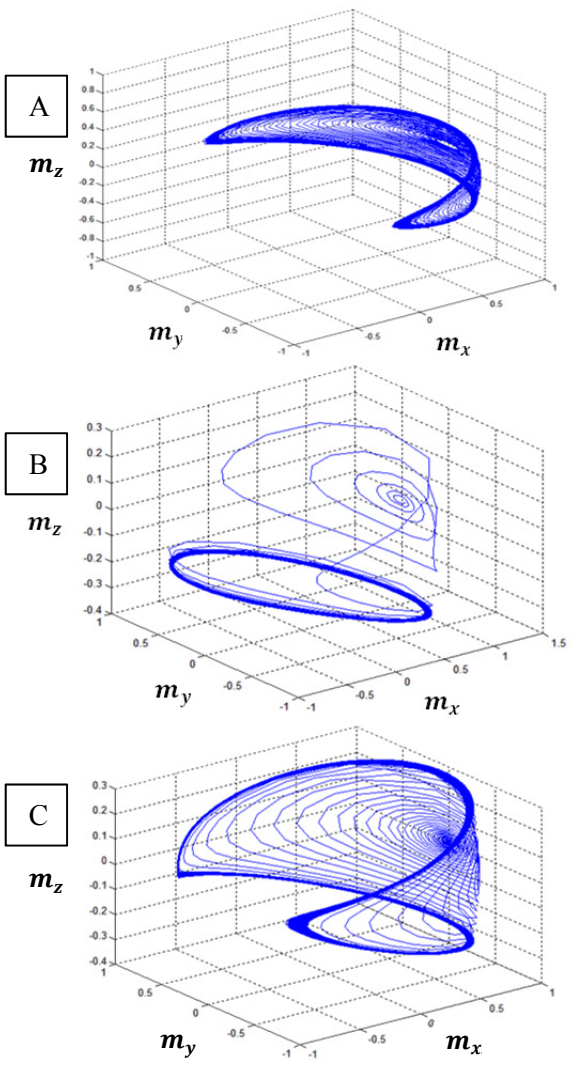

Fig. 3. Magnetization of the free layer ($\hat{m}$) as it goes in to A) in-plane mode, B) out-of-plane mode and C) clam-shape mode of oscillation. The final mode shape forms the outermost thick trajectory where we see steady state precession of magnetization. (A) Frequency of oscillation of in-plane mode is 9.445GHz which was observed at a bias current of 2.1mA. (B) Frequency of oscillation of out-of-plane mode is 7.685GHz which was observed at bias current of 7mA. (C) Frequency of oscillation of the clam-shaped mode is 5.766GHz which was observed at a bias current of 2.85mA.

Effect of the applied AC strain and the resultant locking of the STO can be studied using FFT based frequency spectrum of its modulated impedance ΔR. ΔR at any given time is dependent on the relative directions of magnetization ($\hat{m}$) and the polarizer ($\widehat{ep}$) as shown in (8). Amplitude of ΔR is also determined by the material properties and the device structure but is not relevant for the frequency spectrum analysis. For FFT we consider the data only after intial 60ns which is sufficient time for magnetization to settle into steady state precession and for it to respond to the locking AC strain S, which is turned on 30ns after starting the simulation. Fig. 4 shows the FFT spectrum of different oscillation modes without locking strain in blue and with AC locking strain in red. The relative amplitude of oscillation seen in the blue spectrum across different oscillation modes is reflective of the

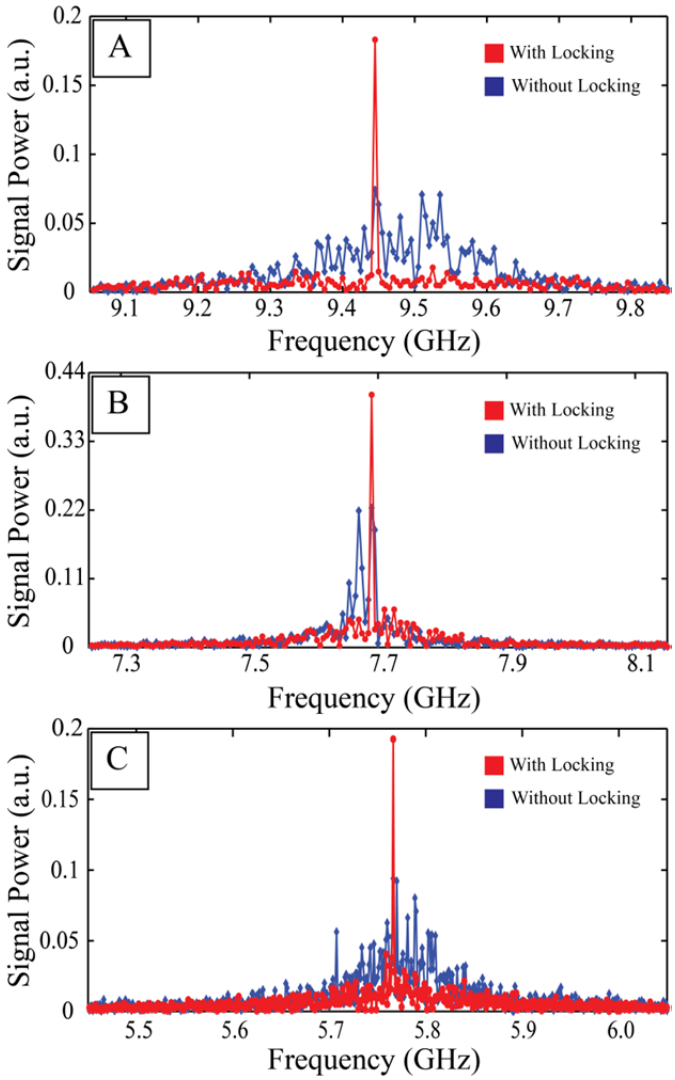

Fig. 4. FFT spectrum of the STO in A) in-plane mode, B) out-of-plane mode and C) clam-shaped mode of oscillation with and without the locking AC strain S.

actual amplitude measured in different experiments [1,3,9]. Specifically the output power of STO increases from in-plane mode (Fig. 4A) to out-of-plane mode (Fig. 4B) with the clam-shaped mode (Fig. 4C) of oscillation having intermediate output power. Higher signal power, narrower linewidth and suppressed suprious modes in the red spectrum compared to the blue spectrum (in Fig. 4) is indicative of the locking of the STO across various modes by the AC strain S from the mecahnical resontor.

The amplitude of the AC strain needed to lock STOs in differents modes of oscillations is shown in Table II. Out-of-plane mode needed 21ppm of AC strain, while in-plane mode

TABLE II. STRAIN AMPLITUDE FOR LOCKING

Oscillation Mode	Locking AC Strain S (ppm)	HBAR Drive (V)
In-Plane	107	4.9
Clam-Shaped	33	2.2
Out-of-Plane	21	1.4

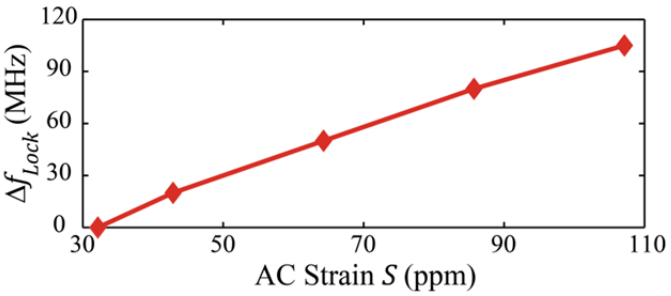

Fig. 5. Locking range of AC strain S as function of its amplitude for the clam-shaped mode of oscillation (shown in Fig. 3C).

required 107ppm. The huge difference in amplitude of strain S is because the magento-acoustic locking field H_{st}, with direction $\hat{t}$, couples into the effective field $\overrightarrow{H_{eff}}$ as a dot product with magnetization $\hat{m}$. For the Z directional strain used in our simulations the amplitude of H_{st} is weighted by the Z component of $\hat{m}$. In in-plane mode of oscillation the magnetization precessesion is mostly along the X-Y plane with a very small Z component, so the locking field amplitude is greatly reduced when it is coupled into the LLGS equation. Hence larger amplitude of AC strain is required for locking in-plane mode compared to out-of-plane or clam-shaped modes, which have larger Z component of magnetization. Table II also shows the voltage drive needed by an AlN HBAR with a silicon substate to generate the locking strain amplitude at the frequency of the STO oscillation. The drive voltage values were calculated using an analytical model for HBAR assuming a quality factor of 1000 and AlN film thickness of half the wavelength [10]. Drive values calculated from the analytical mode are in agreement with finite element analysis done in Comsol.

The locking range of AC strain S for the clam-shaped mode of oscillation with frequency 5.766GHz is shown in Fig. 5. The locking range is linear over an offset frequency range (Δf_{Lock}) of +/− 105MHz for 110ppm amplitude of AC strain S. The limit of locking range, observed as a saturation of the offset frequency, was not seen in our simulations; as we limited our simulations to a maximum strain amplitude of 110ppm, which is very difficult to achieve using HBAR based mechanical strain transducer.

IV. Conclusion

In conclusion, we have demonstrated acoustic locking of Spin Torque Oscillator using a realistic macro-spin model of MTJ with a magneto-elastic coupling term. The model used, takes into account effect of thermal noise and shows the enhancement in linewidth and amplitude of oscillation when subjected to AC locking strain. We have demonstrated locking for various oscillation modes of STO and observe that out-of-plane strain generated by the HBAR is more suited for locking clam-shaped mode or for out-of-plane mode. Acoustic locking illustrated here can be used for synchronizing large number of STOs by locking them to a single mechanical strain transducer. We believe using acoustic locking with HBAR-like transducer in feedback loop with STO an octave frequency tunable hybrid magneto-acoustic oscillator system can be developed.

Acknowledgment

The authors would like to thank the Cornell Center for Materials Research supported by National Science Foundation MRSEC program (DMR-1120296), whose generous grant made this research possible. We also would to thank Dr. Praveen Gowtham for providing measured data on magneto-elastic coupling coefficients of CoFeB-MgO layers and for discussions on acoustic locking and Spin Torque Oscillators.

References

[1] S. I. Kiselev, J. C. Sankey, I. N. Krivorotov, N. C. Emley, R. J. Schoelkopf, R. A. Buhrman, and D. C. Ralph, “Microwave oscillations of a nanomagnet driven by a spin-polarized current,” Nature, vol. 425, no. 6956, pp. 380–383, 2003.

[2] D. C. Ralph and M. D. Stiles, “Spin transfer torques,” J. Magn. Magn. Mater., vol. 320, no. 7, pp. 1190–1216, Apr. 2008.

[3] W. H. Rippard, M. R. Pufall, S. Kaka, T. J. Silva, S. E. Russek, and J. A. Katine, “Injection locking and phase control of spin transfer nanooscillators,” Phys. Rev. Lett., vol. 95, no. 6, p. 067203, 2005.

[4] J. Persson, Y. Zhou, and J. Ä. Kerman, “Phased-locked spin torque oscillators: Impact of device variability and time delay,” J. Appl. Phys., vol. 101, no. 9, pp. 09A503-1–09A503-3, Apr. 2007.

[5] R. C. O’Handley, Modern Magnetic Materials Principle and Applications. New York, NY: Wiley Inter-Science Publication, 2000.

[6] M. Beleggia, M. D. Graef, Y. T. Millev, D. A. Goode, and G. Rowlands, “Demagnetization factors for elliptic cylinders,” J. Phys. D: Appl. Phys., vol. 38, no. 18, pp. 3333–3342, Sep. 2005

[7] W.F. Brown, “Thermal fluctuations of a single-domain particle,” Phys. Rev., vol. 130, no. 5, pp. 1677–1686, Jun. 1963.

[8] L. Liu , C.-F. Pai , D. C. Ralph , and R. A. Buhrman , “Magnetic oscillations driven by the spin Hall effect in 3-terminal magnetic tunnel junction devices,” Phys. Rev. Lett., vol. 109, no. 18, p. 186602, 2012.

[9] Z. Zeng, P. K. Amiri, I. N. Krivorotov, H. Zhao, G. Finocchio, J.-P. Wang, J. A. Katine, Y. Huai, J. Langer, K. Galatsis, K. L. Wang, and H. W. Jiang, “High-Power Coherent Microwave Emission from Magnetic Tunnel Junction Nano-oscillators with Perpendicular Anisotropy,” ACS Nano, vol 6, no.7, pp. 6115–6121, Jun. 2012.

[10] T. A. Gosavi, E. R. MacQuarrie, G. D. Fuchs, and S. A. Bhave, “HBAR as high frequency high stress transducer,” unpublished.